Materials Research. 2025; 28:e20240404
DOI: https://doi.org/10.1590/1980-5373-MR-2024-0404

Processing and Characterization of a Novel ZTA-MgO for Dental Applications

***Ana Clara Bortolucci Saggioro*[a], *Leandro Fernandes*[a], *Mariana de Oliveira Carlos Villas-Bôas*[b], *Rafael Salomão*[c], *Lígia Antunes Pereira Pinelli*[a*]**

[a]*Universidade Estadual Paulista, Faculdade de Odontologia de Araraquara, Departamento de Materiais Odontológicos e Prótese, Araraquara, SP, Brasil.*
[b]*Universidade Federal de São Carlos, Departamento de Engenharia de Materiais, São Carlos, SP, Brasil.*
[c]*Universidade de São Paulo, Escola de Engenharia de São Carlos, Departamento de Engenharia de Materiais, São Carlos, SP, Brasil.*

Received: September 10, 2024; Revised: December 12, 2024; Accepted: January 19, 2025

Zirconia-toughened alumina (ZTA) is a promising material for dentistry; however, its current formulation exhibits a mauve coloration. This study aimed to synthesize a white ZTA ceramic by doping it with 0.7 wt% magnesium oxide (MgO). Specimens (1.2 mm in thickness x 12 mm in diameter) were divided into 3 groups (n = 15): ZTA doped with chromium oxide (ZTA-Cr2O3), ZTA doped with MgO (ZTA-MgO) and ICE-Zirkon (control group). The materials were analyzed using X-ray diffraction, energy-dispersive X-ray fluorescence spectrometer, scanning electron microscopy, and spectrophotometer. Biaxial flexural strength was conducted, and the Weibull modulus (*m*) and probability of failure were calculated. ZTA-MgO group had a white color, showing the pattern for alumina and zirconia grains in ZTA with a typical composition of the materials. It demonstrated superior BFS (915 ±41 MPa) and higher reliability than the ZTA-Cr_2O_3. ZTA-MgO proved to be able to produce white ZTA for future use in dentistry.

Keywords: *Zirconia-toughened alumina, Aluminum Oxide, Zirconium, Magnesium, Flexural Strength.*

1. Introduction

Over the past four decades, dentistry has benefited from the development of ceramic materials[1,2]. Aluminum oxide (or alumina, α-Al_2O_3) was one of the first ceramics used in this field due to its high hardness (20 GPa)[3], biocompatibility, resistance to corrosion, wear, and long-term degradation. However, its limited flexural strength (500 to 650 MPa, 4-point bending test) and lower fracture toughness (K_{IC} = 3 to 4.2 MPa.m$^{1/2}$) led to its replacement in the dental market by zirconia (ZrO_2) partially stabilized by yttrium oxide (Y_2O_3), or 3Y-TZP[4]. The 3Y-TZP family has excellent mechanical properties such as high flexural strength (800 to 1200 MPa, 4-point bending test), fracture toughness (K_{IC} = 6 to 15 MPa.m$^{1/2}$) due to phase transformation strengthening, which reduces crack propagation in the material[4]. In addition, a significant number of monoclinic grains resulting from the toughening process can accelerate long-term degradation[3] and compromise the material by increasing the delamination and chipping rates of the veneering porcelain[5]. Although it has shown great potential in orthopedic medicine, where it is widely used in joint prostheses, its application in dentistry still needs to be improved despite its introduction to this market in 2003[6]. Dental materials must combine aesthetics, durability, and biocompatibility, and while ZTA excels in durability and biocompatibility, it falls short in aesthetics, mainly due to its typical mauve coloration.

ZTA, one of the most researched advanced ceramics in recent times[7], consists of a few individual zirconia grains (ZG) (5 to 30 wt%) dispersed in a compact continuous alumina phase. As a result, any degradation events are confined to minimal zirconia-rich zones that do not affect the alumina matrix. Consequently, the overall life of the structure is extended[8-10]. Its typical mechanical properties are similar to those of 3Y-TZP (1346 MPa, 4-point bending test; 17.25 GPa HV hardness)[11,12], with superior dimensional stability[7] and biocompatibility despite its lower fracture toughness (K_{IC} = 4 to 10 MPa.m$^{1/2}$)[7].

Typical formulations on the market contain up to 0.3 wt% of chromium oxide (Cr_2O_3) as a dopant[13], which imparts a mauve color to the ceramic after heat treatment. The chromium ions are slightly larger than the Al^{3+} ions and replace some of them in the alumina structure, forming an isovalent solution in the crystal lattice[3]. As a result, surface hardness increases, and the overall microstructure is stabilized, protecting the ZG from hydrothermal degradation[14] and extending service life. However, the mauve and blue colors imparted by chromium dopants are aesthetically contraindicated in dentistry. Therefore, an intensive search for new dopants with similar mechanisms and properties[15-18] that do not cause staining of the ceramics has recently begun. Using magnesium oxide (MgO) as a dopant for ZTA structures is an interesting choice. It has already been studied as a component of partially stabilized zirconia[19,20], and it prevents abnormal grain growth in alumina matrices

*e-mail: ligia.pinelli@unesp.br

by pinning grain boundary refinement, thereby improving mechanical strength[20,21]. Therefore, further investigation of zirconia-toughened alumina doped with magnesium oxide (ZTA-MgO) is an exciting prospect.

Although the development and application of novel biomaterials require the evaluation of their properties, one of the most important is flexural strength. According to the EN ISO 6872 standard[22], the flexural strength of ceramics used in prosthetic infrastructures, measured by the 4-point bending test, must be approximately 800 MPa. Therefore, the values of new materials must be close to or higher than this level. This paper describes the preparation and characterization of ZTA-MgO ceramics in terms of their physical properties, such as apparent density, total porosity, flexural strength, and Weibull modulus, which were associated with crystalline phases and microstructure development. Samples designed with Cr_2O_3 as a dopant (ZTA-Cr_2O_3) and simple 3Y-ZrO_2 were also prepared using the same processing methods. The null hypothesis is that the tested groups have no difference in flexural strength and Weibull modulus.

2. Material and Methods

The ZTA-MgO and ZTA-Cr_2O_3 formulations were prepared by combining aluminum oxide (Al_2O_3, A1000SG, Almatis, USA), zirconium oxide (ZrO_2, TOSOH, Japan), magnesium oxide (MgO, Labsynth, Brazil), Chromium oxide (Cr_2O_3, Sigma-Aldrich, USA), Yttrium oxide (Y_2O_3, Sigma-Aldrich, USA), strontium oxide (StXOY, Sigma-Aldrich, USA). The proportions are described in Table 1.

The ICE-Zirkon powder utilized for the reference samples (control group) was obtained by grinding an as-received green block in iron mortar manually and then in a ball mill operated with 5 mm ZrO_2 spheres, a 1:5 spheres-to-powder mass ratio, and a rotation speed of 90 rpm for 72 hours.

The raw materials of each group were combined with polyvinyl butyral (PVB, Sigma, Switzerland, 1 wt%) previously dissolved in isopropanol (Labsynth, Brazil) to create a 33 wt% solids suspension. The material was then homogenized in a ball-mill apparatus (Solab, Brazil) comprising ZrO_2 spheres of 5 mm, a 10:1 spheres-to-powder mass ratio, and a rotation speed of 60 rpm for 72 hours. After that, the material was dried overnight at 60°C and deagglomerated using a 100-mesh sieve. The resulting powders were subjected to uniaxial pressing to create discs with a diameter of 15 mm and a thickness of 1.6 mm. This process was conducted at a pressure of 113 MPa (60 seconds). The discs were subjected to heat treatment in an Infire HTC Speed oven (Sirona Dental Systems GmbH, Germany) at a temperature of 1100°C, at a heating time of 10°C/min, and held for 3 hours, followed by a 10°C/min cooling rate. Finishing operations were conducted using SiC sandpapers ranging from 1200 to 2000 mesh to remove irregularities. Following cleaning and drying, the samples were subjected to sintering (1450°C, 2°C/min heating rate, 3 h hold, 10°C/min cooling rate). For each group, 15 samples (1.2 mm in thickness x 12 mm in diameter) were prepared and tested.

The microstructure of the polished surface was analyzed by scanning electron microscopy (SEM-FEG, JEOL, JSM-7500F, Japan) coupled with an energy-dispersive X-ray fluorescence probe (EDX-720 Shimadzu equipment). Thermal etching was performed at 1400°C for 30 minutes at a heating rate of 5°C/min and a cooling rate of 10°C/min to expose the grain boundary microstructures. Before the assessment, the samples were carbon-coated for 90 seconds at 20 mA using a sputter coater (BAL-TEC SCD 050). The SEM images were imported into image-processing software (Microsoft PowerPoint 2019), and their scale bars were measured to establish a reference point. The grains were measured in 2 axes (major and minor), resulting in an average diameter for each grain. The average grain diameter was defined as the mean value among the 25 measurements.

The crystalline phase composition of each group was identified by X-ray diffraction (D8 Advance ECO; Bruker AXS GmbH, Germany) with $\lambda = 0.15406$ nm, in a 2θ range of 10° to 80°, at a 1° min^{-1} scan rate, using a crushed sample. The proportions of the phases were analyzed using the Rietveld method (software MATCH! version 3.0, Crystal Impact, Germany), adopting the records of the International Centre for Diffraction Data (ICDD). The apparent (AD, g/cm^3) and relative (RD, %) densities and total porosity (TP, %) of the sintered samples were measured using the Archimedes principle and distilled water as the immersion fluid.

The biaxial flexural strength (BFS) was determined by implementing the piston-on-three-ball test per the EN ISO 6872 standard[22], conducted on a universal testing machine (EMIC DL 2000, Instron Brasil Equipamentos Ltda., Brazil) with a 2-kN load cell at a 0.5 mm/min crosshead speed. The specimens were positioned at the apex of 3 steel spheres (2.5 mm in diameter, 120° apart, forming a 10 mm diameter circle). The load was applied perpendicularly to the center of the specimen by a 1.4 mm diameter cylindrical steel piston. Before each test, the dimensions of the individual specimens were measured using a high-precision digital caliper with an

Table 1. Compositions of the ceramics tested.

Raw materials	ZTA-MgO			ZTA-Cr_2O_3			ICE-Zirkon		
	wt%	vol. %	mol %	wt%	vol. %	mol %	wt%	vol. %	mol %
Al_2O_3	75.70	81.29	79.17	75.70	81.07	79.17	-	-	-
MgO	0.70	0.83	1.82	0.00	0.00	0.00	-	-	-
Cr_2O_3	0.00	0.00	0.00	0.70	1.10	0.49	-	-	-
SrO	0.70	0.63	0.71	0.70	0.63	0.72	-	-	-
ZrO_2	22.38	16.80	19.11	22.38	16.75	19.37	94.8	93.8	94 to 96
Y_2O_3	0.53	0.45	0.25	0.53	0.45	0.25	5.2	6.2	4 to 6

accuracy of 0.01 mm. The BFS (σ, in MPa) was calculated using the Equations 1, 2, and 3:

$$X = [(1+\upsilon)\times ln(r_2 / r_3)^2] + [((1-\upsilon) / 2)\times(r_2 / r_3)^2] \quad (1)$$

$$Y = (1+\upsilon)\times[1 + ln(r_1 / r_3)^2 + (1-\upsilon)\times(r_1 / r_3)^2] \quad (2)$$

$$s = -0.2387\times P(X - Y)/b^2 \quad (3)$$

Where P (N) is the breaking load, b (mm) is the thickness of the specimens, ν is the Poisson's radio (0.25), r_1 is the support ball radius (5 mm), r_2 is the radius of the piston tip (0.7 mm), and r_3 is the specimen radius (in mm). The BFS values were subjected to a Shapiro-Wilk normality test (α = 0.05) and the Levene test for homoscedasticity. The data were found to satisfy the assumptions of normality and homoscedasticity and were analyzed by one-way ANOVA in a software program (PRISMA, GraphPad Software, USA), with α = 0.05; it was also conducted the Dunnett pos-hoc test.

The Weibull modulus (*m*, dimensionless, ranging from zero up to infinity) was calculated by the guidelines EN ISO 6872[22]. The results were initially ranked in ascending order and plotted against the accumulated probability of failure (P_f), which was determined by Equation 4:

$$P_f(\sigma_i) = (i - 0.5) / N \quad (4)$$

Where i is the specimen rank according to its fracture strength, and N is the total number of specimens tested. The values of Weibull modulus were then calculated and deduced using linear regression with Equation 5, where σ_0 is the characteristic stress.

$$ln.ln(1/1-Pf) = m.ln\sigma - mln\ \sigma_0 \quad (5)$$

Equation 6 calculated confidence intervals from a limited number of measurements (*n*) with a mean ($\bar{x}$) and sample standard deviation (s).

$$Confidence\ interval = \bar{x} \pm (ts/\sqrt{n}) = \bar{x} \pm tu_x \quad (6)$$

Where: *t* is Student's t, for 95% confidence level. The expression on the right replaces the standard deviation of the mean with an equivalent quantity u_x, called standard uncertainty.

Three readings of the color coordinates (L*, a*, and b*) of the CIELAB system were conducted on a single specimen from each group using a spectrophotometer (Easyshade, Vita, Zahnfabrik, Germany; illuminant D55; temperature 5500K; angle of measurement 0°). The measurements were taken on a black background. L* represents perceptual lightness, a*, the spectrum of color from green to red, and b*, the spectrum of color from blue to yellow. The device was set to the "basic color measurement" function, with the active tip positioned in the center of the sample and close contact with the specimen.

3. Results and Discussion

In contrast to the ICE-Zirkon samples, which exhibited a smooth granular microstructure with grain diameters ranging from 0.15 µm to 1 µm (Figure 1a) and high densification (Figure 1b), the ZTA-Cr_2O_3 samples displayed a rougher morphology, with ZG and alumina grains (AG) exhibiting a range of sizes (Figure 1c). Additionally, it shows the formation of agglomerates of ZG and AG, as well as a reduction in densification, as indicated by the presence of residual porosity (Figure 1d). In the ZTA-MgO composition, the ZG are observed to be more dispersed and individualized than in the ZTA-Cr_2O_3 group, within a highly densified microstructure. Figures 1e and 1f illustrate the ZTA-MgO group, which features AG and ZG measuring approximately 1.08 µm 0.36 µm, respectively. These observations are similar to those in the ZTA-Cr_2O_3 group but exhibit a superior distribution of ZG along the alumina contours, indicating a denser packing of AG by zirconia compared to the chromium group. These results indicate that the AG is better packed by the zirconia than by the group with chromium, and this morphology is essential to the mechanical performance of the material[23].

Table 2 presents the semi-quantitative results of the EDXRF spectrometry of the ceramic materials. The ICE-Zirkon sample exhibited a yttrium oxide content of 5.5 wt% and a zirconium oxide content of 94.5 wt%, indicating a mass difference of 0.3% compared to the 3Y-TZP compositions, which is consistent with the large-scale production process. The ZTA samples displayed compositions comparable to the groups' additions (Table 1).

Upon examination of the FEG-SEM images of each group, it was observed that the ZTA-Cr_2O_3 exhibited a prevalence of superficial pores and an unorganized microstructure. The AG was less well-packed than the ZG, as seen in the magnesium-added group. This resulted in a greater mechanical fragility of the latter group, reflected in the low flexural strength results. In contrast, the ZTA-MgO exhibited an organized microstructure consistent with other researchers' findings[6,14,16,17,20]. This structure involved ZG (lighter in atomic weight) situated between matrix alumina plates (darker in atomic weight) (Figure 1). Singh et al.[23] asserted that the toughness mechanism of ZTA is contingent upon the zirconia grain size, phase, and location within the alumina matrix, which are all directly influenced by the sample preparation method. The uniformity of the grains in the ZTA-MgO group can be attributed to the presence of magnesium oxide during its processing, as this helps to control the growth of AG, thus improving the mechanical quality of the material[8,9,15,16,24].

Figure 2 depicts the phase analysis conducted by XRD, and Table 3 shows the quantification performed by the Rietveld method. Figure 2a illustrates zirconia's tetragonal and cubic phases within the Ice-Zirkon group, with Table 3 indicating the respective proportions of 65.8 wt% and 34.2 wt% for each. As anticipated, the monoclinic phase was not identified, suggesting that it is stabilized in the tetragonal and cubic phases. The presence of a monoclinic phase (6.7 wt%) observed in ZTA-Cr_2O_3 is indicative of a phase transition. In comparison, ZTA-MgO exhibited a lower amount of the monoclinic phase (3.9 wt%) and the highest amount of the tetragonal phase (9.4 wt%). The ZTA groups demonstrated an 84.9 to 85.1 wt% range of alumina (Table 3). The patterns observed in X-ray diffraction indicate that ZTA-MgO has approximately 2/3 of its composition in tetragonal and cubic phases compared to the monoclinic phase. In contrast, ZTA-Cr_2O_3 shows a ratio (t+c:m) of approximately 1:1, suggesting it may have greater resistance than the former. This finding aligns with the observed higher resistance of ZTA-MgO.

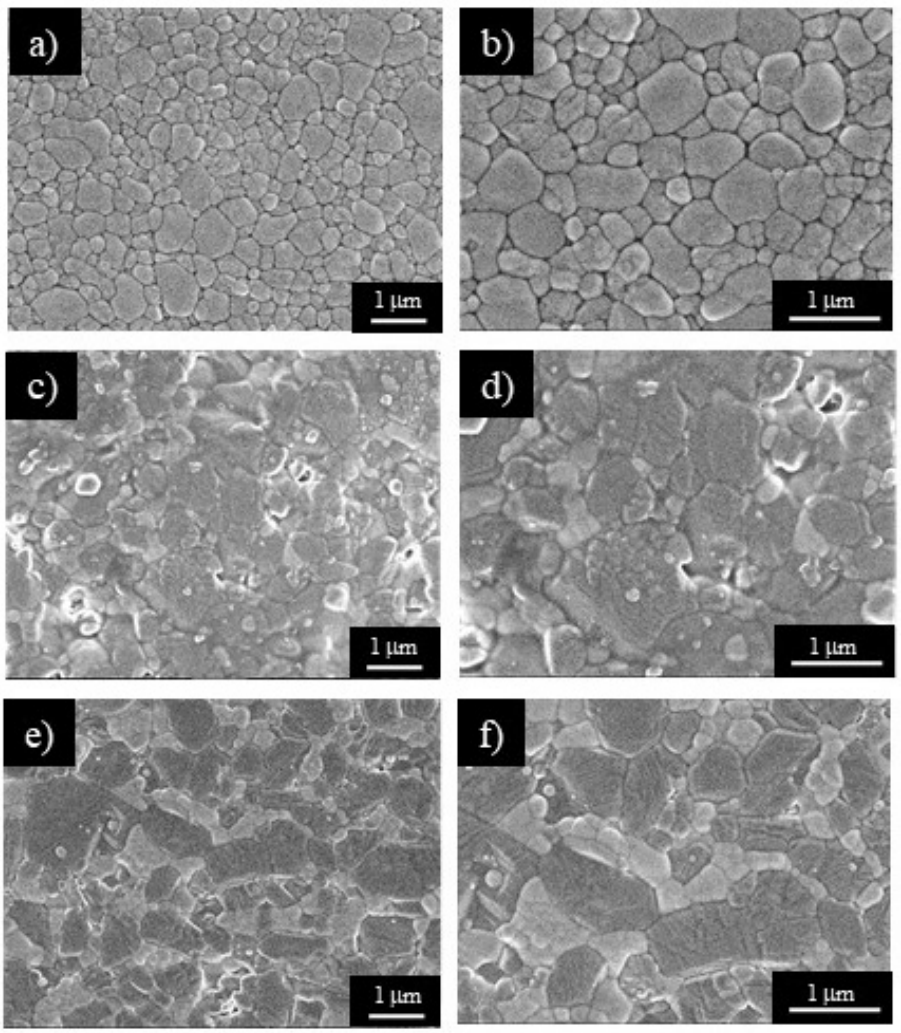

Figure 1. Scanning electron microscopy images of the surfaces of specimens after heat treatment: a-b) ICE-Zirkon, c-d) ZTA-Cr_2O_3, and e-f) ZTA-MgO. The alumina grains appear as darker phases, whereas the zirconia ones are brighter due to the atomic number contrast.

Table 2. EDXRF analysis of ICE-Zirkon, ZTA-Cr_2O_3, and ZTA-MgO groups.

Elements	Compositions tested		
	ICE-Zirkon	ZTA-Cr_2O_3	ZTA-MgO
	(wt%)	(wt%)	(wt%)
Alumina oxide	0	75.18	74.08
Zirconium oxide	94.50	22.93	24.22
Yttrium oxide	5.50	1.21	1.27
Chromium oxide	0	0.96	0
Magnesium oxide	0	0	0.42

Table 3. Quantification of the crystalline phases for each experimental group.

Crystalline phases	ICE-Zirkon (wt%)	ZTA-Cr_2O_3 (wt%)	ZTA-MgO (wt%)
Tetragonal ZrO_2	65.8	7.0	9.4
Monoclinic ZrO_2	0.0	6.7	3.9
Cubic ZrO_2	34.2	1.4	1.6
α-Al_2O_3	0.0	84.9	85.1

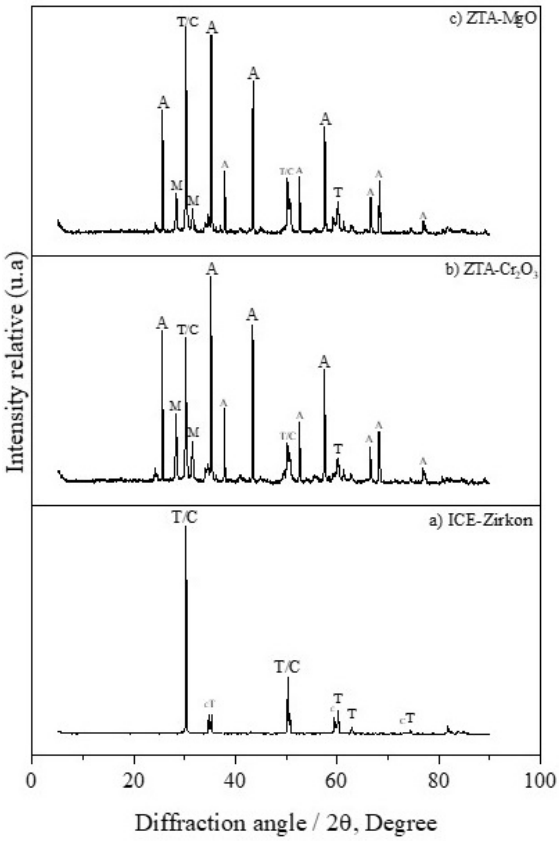

Figure 2. X-ray diffraction pattern for a) ICE-Zirkon, b) ZTA-Cr_2O_3, and c) ZTA-MgO samples. List of symbols (ICDD files): T: tetragonal ZrO_2 (96-152-1475), C: cubic ZrO_2 (96-210-1235), M: cubic ZrO_2 (96-152-1754), A: α-Al_2O_3 (96-900-9672).

The ICE-Zirkon exhibited the highest degree of densification, reaching 98.87% of apparent density and 1.13% of total porosity, and a lower porosity than the ZTA groups. The ZTA-Cr_2O_3 sample exhibited a total porosity of 4.09%, which is lower than that observed in the ZTA-MgO sample (6.17%) (Table 4).

Although the total porosity level of ZTA-MgO (6.17%) was higher than that observed for other groups, it did not exert a significant negative mechanical effect on the group. It has been reported that the inclusion of MgO has been observed to lead to the formation of secondary phases such as spinel ($MgAl_2O_4$) and MgO, which are comparatively softer. However, despite its inherent softness, MgO has the potential to enhance toughness by absorbing crack energy. This finding has been documented by other authors[8,9,20]. Consequently, despite exhibiting higher porosity and lower density, ZTA-MgO demonstrated superior mechanical properties. The transformation t-m may result in tensile stress on ICE-Zirkon due to the accumulation of compressive stress during the BFS test. The grains in ZTA-MgO are unlikely to collapse because of the volumetric increase in porosity, which may be insufficient for a critical tension, as stated by Lopes et al.[18]. The ZTA with MgO obtained favorable mechanical results due to its microstructural characteristics, attaining up to 80% of the expected properties and with a whitish appearance, which suggests that it could be a promising rehabilitative material.

Table 4. Mean and standard deviation of total porosity (%), apparent density (g.cm^{-3}) and relative density (%) results for ICE-Zirkon, ZTA-Cr_2O_3, and ZTA-MgO samples.

Material	ICE-Zirkon	ZTA-Cr_2O_3	ZTA-MgO
Total porosity	1.13 ±0.04	4.09 ±1.4	6.17 ±2.0
Apparent density	5.93 ±0.26	4.23 ±0.20	4.13 ±0.12
Relative density	98.87	95.90	93.83

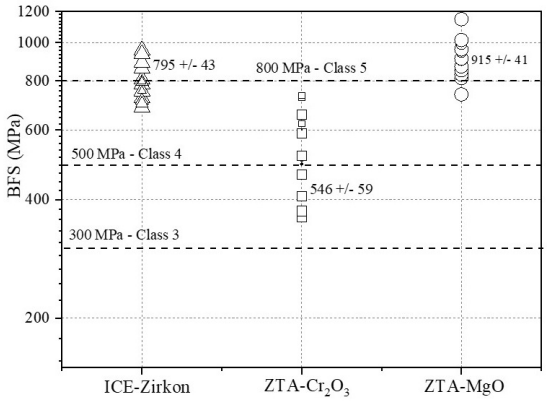

Figure 3. The biaxial flexural strength of the ICE-Zirkon, ZTA-Cr2O3, and ZTA-MgO samples is presented. The horizontal dotted lines represent the typical results for dental restoration as defined in ISO 6872[22].

Figure 3 illustrates the outcomes of the BFS assessment of the ceramic materials under examination. The statistical analysis revealed a statistically significant discrepancy between the groups ($p < 0.0001$).

The highest resistance value was observed for the ZTA-MgO group (915 ±41 MPa, CI 95%), followed by ICE-Zirkon (795 ±43 MPa, CI 95%), which exhibited a similar trend to that reported in the literature[25,26]. The mechanical results of ZTA-Cr_2O_3 achieved in this study (546 ±59 MPa, CI 95%) were not comparable to the results of the market-available product (1346 MPa). This discrepancy is likely attributable to the technique used for the heat treatment. The hot isostatic pressing (HIP) technique, as employed by Kuntz[11], involves heating the material to 1400 °C under high isostatic pressures. This process effectively reduces the porosity of the material while enhancing its mechanical properties. However, in this study, the ZTA-Cr_2O_3 HIP was not utilized as a pressing technique, resulting in a total porosity of 4.09%.

The organization of this material's microstructure is a critical determinant of its mechanical behavior. Studies have demonstrated that dopants that enhance the formation of plate-like grains within the microstructure can facilitate crack deflection, thereby strengthening the material[20,27]. Consequently, the mechanical outcomes are closely linked to the organization of the microstructure, as evidenced by the FEG-SEM images.

Figure 4 illustrates the reliability of the materials and the discrepancies in BFS for a 63.2% P_f. Weibull modulus values were m = 10.63 for the ICE-Zirkon, m = 5.42 for ZTA-Cr_2O_3, and m = 10.49 for ZTA-MgO. The value for

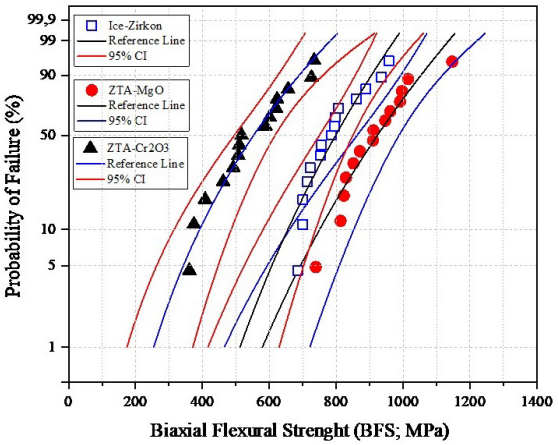

Figure 4. Weibull statistical analysis, stress-strain curves for Ice-Zirkon, ZTA-MgO, and ZTA-Cr_2O_3, showing reference lines and 95% confidence intervals for each material.

Figure 5. ICE-Zirkon (left), ZTA-Cr_2O_3 (middle), and ZTA-MgO (right) specimens.

Table 5. CIELAB coordinates for ICE-Zirkon, ZTA-Cr_2O_3, and ZTA-MgO samples.

Groups	ICE-Zirkon	ZTA-Cr_2O_3	ZTA-MgO
L*	80.7333	13.4667	28.1667
a*	-1.0333	7.7000	3.2667
b*	7.1000	7.4333	12.5000

ZTA-MgO was higher than that for ZTA-Cr_2O_3 and nearly identical to that for the control group. ZTA-MgO exhibited superior mechanical resistance and a higher probability of survival under identical operational conditions than the other groups.

The *m* is a critical parameter in dentistry for assessing the reliability and predictability of dental materials, particularly in restorative and prosthetic applications; a higher *m* correlates with a lower P_f over time. It indicates less variability in the strength of the material, meaning the material is more predictable and consistent in its performance, contributing to the long-term success of treatments[17]. It is essential to ensure that dental restorations and prostheses can withstand masticatory forces without unexpected failure, indicating less variability in the strength of the material, meaning the material is more predictable and consistent in its performance. Figures 4 show that the *m* and the P_f corroborate with other results, in which the ZTA-MgO and ICE-Zirkon show values of *m* next to each other, respectively, which indicates that ZTA-MgO is a material reliable for the infrastructure of dental prostheses regarding mechanical aspect such result is similar to those observed by Benalcazar Jalkh et al.[17] which compared a ZTA with 0.1 wt% magnesium oxide and dental zirconia and observed better mechanical results for ZTA, especially after artificial aging, thus indicating the material may be a good option for use as dental prostheses. It can be observed in Figure 4 that the lines corresponding to the 95% confidence interval for ZTA-MgO and ICE-Zirkon intersect at specific points, indicating a statistical similarity between these compositions. The confidence interval for ZTA-Cr_2O_3 does not overlap with any other composition.

Table 5 illustrates the mean coordinates of each group according to the CIELAB. The ZTA-Cr_2O_3 specimen exhibits a positive and high value for the a* coordinate, indicating that it possesses a reddish color that is more pronounced than the other specimens. Figure 5 shows the color of specimens of the ZTA-MgO, ICE-Zirkon, and ZTA-Cr_2O_3 groups after sintering.

Spectrophotometric analysis is a non-invasive method used to measure the color of dental materials and teeth by quantifying the intensity of light reflected or transmitted. It ensures consistent, objective, and accurate evaluation of color, which is crucial for aesthetic dental restorations. The L*, a*, and b* parameters are derived from the CIELAB color space, where L* represents lightness, ranging from 0 (black) to 100 (white)[28]. It determines the brightness or darkness of dental material or tooth; a* measures the green-red axis; a positive value indicates redness, while a negative value indicates greenness, which is important to assess the redness of gums or restorations. Moreover, b* measures the blue-yellow axis; positive values indicate yellowness, while negative values indicate blueness. This parameter is critical for evaluating enamel and dentin shades[28].

The spectrophotometry results indicate that ZTA-MgO is in CIELAB coordinates closer to the center of the CIELAB diagram than ZTA-Cr_2O_3. Despite its L* coordinate being lower than that of ICE-Zirkon, it is observed to be higher than that of ZTA-Cr_2O_3, suggesting that this group exhibits more remarkable similarity to ICE-Zirkon than ZTA-Cr_2O_3.

The findings of this study indicate a need for further research to accelerate improvements in ZTA when replacing the chromium oxide dopant with magnesium oxides. It would be beneficial to investigate how the behavior towards fatigue and hydrothermal aging affects the characteristics of ZTA-MgO and other properties such as aesthetic characteristics, dimensional stability, and adhesion of this material with veneering porcelain and a dental substrate.

4. Conclusions

Incorporating magnesium oxide (MgO) into zirconia-toughened alumina (ZTA) ceramics has yielded promising outcomes, particularly regarding mechanical reliability for dental prostheses infrastructure. Our study corroborates previous findings, emphasizing the favorable performance of ZTA-MgO compared to ZTA-Cr_2O_3 and its proximity to ICE-Zirkon in CIELAB coordinates. These results highlight the potential of ZTA-MgO as a viable alternative for dental prostheses.

5. Acknowledgments

The authors acknowledge the Brazilian Research Foundations FAPESP (2010-19274-5; 2017/06738-2; 2018/19773-3), CAPES (Finance Code 001), and CNPq (305877/2017-8) for supporting this research; and Almatis (Brazil and USA) for the samples of calcined alumina. They also thank Bruno A. Mascaro for spectrophotometry and Pedro Braga for the biaxial flexural strength tests.

6. References

1. Chevalier J. What future for zirconia as biomaterial? Biomaterials. 2006;27(4):535-43.
2. Gremillard L, Tadier S. Materials of hard tissues applications: an overview. In: Palmero P, Cambier F, Barra E, editors. Advances in ceramics biomaterials: materials, devices and challenges. Cambridge: Elsevier; 2017. p. 9-11.
3. Kuntz M, Krüger R. The effect of microstructure and chromia content on the properties of zirconia toughened alumina. Ceram Int. 2018;44:2011-20.
4. Ducheyne P, Healy KE, Grainger DW, Hutmacher DW, Kirkpatrick CJ. Comprehensive biomaterials: Metallic, Ceramic and Polymeric Biomaterial. Amsterdam: Elsevier; 2011.
5. Denry I, Kelly JR. State of the art of zirconia for dental applications. Dent Mater. 2008;24(3):299-307.
6. Piconi C. Ceramics for joint replacement: design and application of commercial bearings. In: Palmero P, Barra E, Cambier F, editors. Advances in Ceramic Biomaterials: Materials, Devices and Challenges. Duxford: Elsevier; 2017. p 129-79.
7. Sarker S, Mumu HT, Al-Amin M, Alam MZ, Gafur MA. Impacts of inclusion of additives on physical, microstructural, and mechanical properties of Alumina and Zirconia toughened alumina (ZTA) ceramic composite: A review. Mater Today Proc. 2022;62(6):2892-918.
8. Rejab NA, Zahirani A, Azhar A, Ratnam MM, Ahmad ZA. The relationship between microstructure and fracture toughness of zirconia toughened alumina (ZTA) added with MgO and CeO2. IJRMHM. 2013;41:522-30.
9. Rejab NA, Azhar A, Ratnam MM, Ahmad ZA. The effects of CeO2 addition on the physical, microstructural and mechanical properties of yttria stabilized zirconia toughened alumina (ZTA). IJRMHM. 2014;36:162-6.
10. Sequeira S, Fernandes MH, Neves N, Almeida MM. Development and characterization of zirconia-alumina composites for orthopedic implants. Ceram Int. 2016;43:693-703.
11. Kuntz M. Live-time prediction of BIOLOX® delta. In: Ceramics in Orthopaedics: Bioceramics and Alternative Bearings in Joint Arthroplasty; 12th International BIOLOX Symposium. Proceedings. Darmstadt: Steinkopff; 2007. p 281-8.
12. Piconi C, Streicher RM. Forty years of ceramic-on-ceramic THR bearings. Semin Arthroplasty. 2013;24:188-92.
13. Xia JF, Nian HQ, Liu W, Wang XG, Jiang DY. Effect of Cr2O3 derived from Cr(NO3)3·9H2O precursor on the densification and mechanical properties of zirconia-toughened alumina (ZTA) composites. Ceram Int. 2016;42(7):9116-24.
14. Pezzotti G, Munisso MC, Porporati AA, Lessnau K. On the role of oxygen vacancies and lattice strain in the tetragonal to monoclinic transformation in alumina/zirconia composites and improved environmental stability. Biomaterials. 2010;31(27):6901-8.
15. Tang D, Lim HB, Lee KJ, Lee CH, Cho WS. Evaluation of mechanical reliability of zirconia-toughened alumina composites for dental implants. Ceram Int. 2012;38(3):2429-36.
16. Rejab NA, Lee WK, Sktani ZDI, Ahmad ZA. Hardness and toughness enhancement of CeO2 addition to ZTA ceramics through HIPping technique. Int J Refract Met Hard Mater. 2017;69:60-5.
17. Benalcazar Jalkh EB, Monteiro KN, Cesar PF, Genova LA, Bergamo ETP, Lopes ACO, et al. Aging resistant ZTA composite for dental applications: microstructural, optical and mechanical characterization. Dent Mater. 2020;36(9):1190-200.
18. Lopes ACO, Jalkh EBB, Bergamo ETP, Genova LA, Bergamo ET, Oliveira Lopes AC, et al. Development of ZTA (80% Al_2O_3/20% ZrO_2) pre-sintered blocks for milling in CAD/CAM systems. J Mech Behav Biomed Mater. 2020;36(12):365-74.
19. Mahmood AA, Gafur MA, Hoque ME. Effect of MgO on the physical, mechanical, and microstructural properties of ZTA-TiO2 composites. Mater Sci Eng A. 2017;707:118-24.
20. Arab A, Zhou Q, Ahmad Z, Chen P, Sktani Z. Effect of MgO addition on mechanical and dynamic properties of Zirconia toughened Alumina (ZTA) ceramic. Materials (Basel). 2019;12(15):2440.
21. Bae IJ, Baik S. Abnormal grain growth of alumina. J Am Ceram Soc. 1997;80:1149-56.
22. International Organization for Standardization. ISO 6872:201: Dentistry: ceramic materials. Geneve: ISO; 2015.
23. Singh BK, Roy H, Mondal B, Roy SS, Mandal N. Development and machinability evaluation of MgO doped Y-ZTA ceramic inserts for high-speed machining of steel. Mach Sci Technol. 2018;22(6):899-913.
24. Jalkh EB, Coelho PG, Witek L, Bergamo ETP, Lopes ACDO, Monteiro KN, et al. Nanoscale physico-mechanical properties of an aging resistant ZTA composite. J Mech Behav Biomed Mater. 2021;123:104690.
25. Adabo GL, Mariscal EM, Hatanaka GR. Flexural strength and microstructure of anterior/monolithic zirconia after low-temperature aging. Dent Mater. 2015;31:48-9.
26. Candido LM, Miotto LN, Fais LMG, Cesar PF, Pinelli LA. Mechanical and surface properties of monolithic zirconia. Oper Dent. 2018;43(3):E119-28.
27. Naga SM, Elshaer M, Awaad M, Amer AA. Strontium hexaaluminate/ZTA composites: preparation and characterization. Mater Chem Phys. 2019;232:23-7.
28. Melo CBF, Feitosa MD, Maia SDB, Barreto JO, Peixoto RF, Regis RR. Effect of a continuous mechanical polishing protocol on the color stainability, microhardness, mass, and surface roughness of denture base acrylic resin. J Prosthet Dent. 2021;126(6):796-802. http://doi.org/10.1016/j.prosdent.2020.06.007.